

ROBUST QUANTIFICATION OF PULMONARY EMPHYSEMA WITH A HIDDEN MARKOV MEASURE FIELD MODEL

Yrjö Häme¹, Elsa D. Angelini^{1,2}, Eric A. Hoffman³, R. Graham Barr⁴, Andrew F. Laine¹

¹Department of Biomedical Engineering, Columbia University, New York, NY, USA

²Institut Mines-Telecom, Telecom ParisTech, LTCI CNRS, Paris, France

³Department of Radiology, University of Iowa, Iowa City, IA, USA

⁴Department of Medicine, College of Physicians and Surgeons, Columbia University, NY, NY, USA

ABSTRACT

Determining the extent of pulmonary emphysema with quantitative computed tomography commonly relies on fixed intensity threshold values. However, the reliability of such measures is limited due to variability in parenchymal intensities and noise levels in CT images. In this work, we present a novel method for emphysema quantification, based on a lung tissue segmentation with a Hidden Markov Measure Field model. By adapting to the intensity distribution present in the input image, the method provides a more robust emphysema index than standard densitometric approaches. The focus of this study is to show robustness between imaging protocols, enabling the comparison of emphysema measures between studies. The method can have a significant impact in longitudinal analysis and prediction of emphysema. In addition, the method shows promise in delineating emphysematous regions, potentially facilitating subtyping of the disease.

Index Terms— Emphysema, Markov field, segmentation

1. INTRODUCTION

Parenchymal destruction in the lungs, or *emphysema*, is a condition involving alveolar wall destruction [1]. A mixture of emphysema and small airways disease contributes to chronic airflow limitation characteristic of chronic obstructive pulmonary disease (COPD), which is a leading cause of morbidity and mortality worldwide [2].

Computed tomography (CT) is commonly used to identify and quantify the extent of pulmonary emphysema. Generally, an estimate of emphysema severity is obtained using a densitometric measure, called the *emphysema index (EI)* (also referred to as *percent emphysema* or *percent low attenuation area*), which quantifies the proportional area of image points with intensities below a fixed threshold within the lung region. The *EI* is commonly used in clinical COPD studies,

but there is no consensus on the intensity threshold value that should be used and the values typically range from -950 to -910 Hounsfield Units (HU) (see review in [3]).

EI values are obviously influenced by the choice of the intensity threshold, but also by several other factors that cause variation in the level of noise and parenchymal intensity level present in CT images. These factors include the image reconstruction algorithm, slice thickness, scanner type and calibration, radiation dose, gravity and inspiration level [1]. Recent studies have proposed to normalize the resulting *EI* to account for differences between reconstruction algorithms and slice thickness [4, 5]. However, these approaches only consider a part of the sources of variation and have the shortcoming of only adapting the final *EI* score, not the original selection of pixels. In terms of image processing, texture-based analysis of emphysema [6, 7, 8] has been studied to take spatial information into consideration, but these approaches require labeled data to train classifiers, and have not been shown to be robust to changes in imaging protocols.

In this work, we propose a novel method for emphysema quantification based on a segmentation of lung tissue using a Hidden Markov Measure Field (HMMF) model [9]. This approach has two benefits compared to existing approaches: 1) the appearance model adapts to the image data, providing robustness with respect to variability in intensity distributions, and 2) the Markov field enforces spatial coherence of the segmented regions, providing robustness with respect to noise. We demonstrate that the proposed segmentation not only produces robust measures of *EI*, but also robust delineations of diseased regions, which can be useful in determining subtypes of emphysema. The HMMF model has been used in our previous work for liver tumor segmentation [10].

2. METHODS

2.1. Data and Preprocessing

The CT data used in this study included 22 subjects from the EMCAP data set [11]. All subjects underwent low-dose, non-contrast, full-lung CT scanning on a Siemens 16 multidetector

Yrjö Häme is funded by the International Fulbright Science and Technology Award at the U.S. Department of State. Additional funding provided by NIH/NHLBI R01s HL075476, HL077612 and HL083091.

scanner (120 kVp, 169 mAs, 6:1 pitch, 0.75 mm slice thickness, single breath-hold). For each acquisition, three different reconstructions were used, with convolution kernels B31f, B46f, and B60f.

Lungs and large airways were segmented using an approach similar to [12], by applying an intensity threshold of -400 HU and then locating the largest connected objects in the resulting binary volume. The trachea and some of the large airways were then separated from the lungs by using closed space dilation [13].

Threshold-based EI measures were computed for three different thresholds: -980 HU, -950 HU and -910 HU. The respective indices are denoted as EI_{-980}^R , EI_{-950}^R , and EI_{-910}^R , where $R \in \{31, 46, 60\}$ indicates the image reconstruction kernel. All EI values are expressed in percentages.

2.2. Segmentation with the HMMF model

A two-class HMMF model was used to segment lung tissues and quantify emphysema. Let I denote the input image, Ω represents the image domain, and $r \in \Omega$ is an image point. The segmentation process involves two steps. The first step computes a continuous-valued Markov random vector field $q = [q_1, q_2]$, and the second step generates a binary label field f from q . The vector field q represents an intermediate labeling and is assigned a distribution

$$P_q(q) = \frac{1}{K} \exp \left[- \sum_C W_C(q) \right], \quad (1)$$

where C are spatial cliques of the selected neighborhood system, W_C are potential functions and K is a positive normalizing constant. The vector field q has the additional constraint: $q_1(r) + q_2(r) = 1$, $q_1, q_2 \geq 0$, where $q_k(r)$ is the value corresponding to class k at point r . Here, 3D pairwise cliques in 26-connected neighborhoods were used. The potential functions were defined as (similarly to [10]):

$$W_{r_1 r_2}(q) = \lambda \exp \left[- \frac{d(r_1, r_2)^2}{2\sigma_W^2} \right] \sum_{k=1}^2 (q_k(r_1) - q_k(r_2))^2, \quad (2)$$

where $d(r_1, r_2)$ corresponds to the Euclidian distance between the two points (r_1, r_2) , and σ_W and λ are weighting constants. Selection of the values for these parameters is discussed in Section 2.3.

The posterior distribution for q and the associated parameter vector $\theta = [\theta_1, \theta_2]$ is obtained from the Bayes rule:

$$P(q, \theta | I) = \frac{1}{Z} P(I | q, \theta) P_q(q) P_\theta(\theta), \quad (3)$$

where Z is a positive normalizing constant. Each θ_k represents the mean of a Gaussian distribution v_{θ_k} for class k . The prior distribution $P_\theta(\theta)$ was assigned a Gaussian distribution with respect to θ_1 , with standard deviation of 40, centered at

-1000 HU, which corresponds to the value of air. $P_\theta(\theta)$ was constant with respect to θ_2 , to provide adaptivity.

The likelihood function can be represented as [9]: $P(I(r) | q, \theta) = v_{\theta_1}(r)q_1(r) + v_{\theta_2}(r)q_2(r)$. Combining (1) and (3), the measure field is found as a *maximum a posteriori* (MAP) estimate of $P(q, \theta | I) = \frac{1}{KZ} \exp [-U(q, \theta)]$, where

$$U(q, \theta) = - \sum_{r \in \Omega} \log [v_{\theta_1}(r)q_1(r) + v_{\theta_2}(r)q_2(r)] + \sum_C W_C(q) - \log(P_\theta(\theta)). \quad (4)$$

Since $KZ > 0$, the MAP estimates q^* and θ^* for q and θ are found by minimizing $U(q, \theta)$. The optimization was performed with the gradient projection Newtonian descent, as formulated in [9]. Finally, a binary label $f(r)$ for point r is defined as $f(r) = 1$ if $q_1^*(r) > q_2^*(r)$, and $f(r) = 2$, otherwise. To complete the segmentation model description, the following subsection describes how the values for the parameters λ and σ_W were selected. The EI from the proposed method are denoted as EI_{MF}^R .

2.3. Parameter selection

The Markov field weight λ determines how much influence neighboring values of the measure field q have at each point. This value should be chosen according to the noise level of the image. To find an optimal λ^R value for a given reconstruction R , the EI_{MF}^{31} was first computed using an arbitrary small weight value, $\lambda^{31} = 0.1$ (B31f being the smoothest reconstructions in the used data set). The resulting scores were then used as reference values for the noisier reconstructions of the same subject, with λ values tested between 1.0 and 6.0, with increments of 0.5. Increasing λ caused EI_{MF} to decrease without exception, justifying the value range that was tested.

The parameter σ_W defines how fast the Markov weight decreases as a function of voxel distance, and is critical when considering 3D neighborhoods. The same value $\sigma_W = 1.5$ as in [10] was used.

3. RESULTS

For EI_{MF}^{46} and EI_{MF}^{60} , the smallest mean absolute differences (MAD) between EI_{MF}^{31} , over all subjects, were found at $\lambda^{46} = 2.0$ ($MAD = 1.1$), and $\lambda^{60} = 4.5$ ($MAD = 2.1$), respectively. Out of the 22 subjects, the smallest absolute difference to the corresponding EI_{MF}^{31} was obtained within range $\lambda^{46} = [1.5, 2.5]$ for 19 subjects, and within $\lambda^{60} = [3.5, 5.5]$ for 18 subjects. The MAD values with standard deviations as a function of λ are shown in Fig. 1.

The obtained EI_{MF} were compared to the thresholding-based measures for different reconstructions. The mean values, standard deviations, minimum and maximum values of

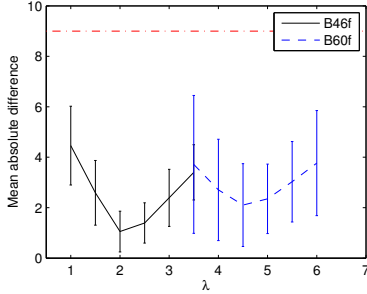


Fig. 1. Mean absolute differences (MAD) and standard deviations between EI_{MF}^{31} and: EI_{MF}^{46} (solid) and EI_{MF}^{60} (dashed) for different values of λ , over 22 subjects. For comparison, the horizontal line represents the observed $MAD = 9.0$ between EI_{-950}^{31} and EI_{-950}^{46} for the same data.

EI for the different quantification methods over the 22 subjects used in the study are reported in Table 1. Figure 2 shows an example of the delineations of emphysema regions for a single subject with the different methods. The effect of noise on the thresholding-based delineations is apparent, while the HMMF-based method delineates the emphysematous regions fairly consistently across the different reconstructions.

Compared to the mean of EI_{-950} , the mean of EI_{MF} was slightly higher for B31f images, and lower for the noisier images. The inter-subject variability (i.e. standard deviation) of EI_{MF} was lower than that of EI_{-950} for all reconstructions, partially due to the narrower range of values in EI_{MF} .

The differences in EI between different reconstruction kernels are reported in Table 2. As expected, the differences for the thresholding-based measures increased with noise, while the proposed quantification method was able to adapt to the noise levels in the images and provided steady responses. The MAD to the reference image (1.1 for B46f, 2.1 for B60f) can be considered small when compared to corresponding differences between the thresholding-based EI values. As seen in Fig. 1, selecting a proper value for λ is an important aspect of the segmentation model, since it has a clear effect on EI_{MF} . Still, for λ values within the range that was tested for this analysis, the differences in EI_{MF} values were well below the corresponding differences for thresholding-based approaches.

For the thresholding approaches, the mean (signed) differences of EI between reconstruction kernels were equal to MAD values. For EI_{MF} , the mean differences between $[EI_{MF}^{31}, EI_{MF}^{46}]$ and between $[EI_{MF}^{31}, EI_{MF}^{60}]$ were 0.6 and 0.3, respectively.

4. DISCUSSION AND FUTURE WORK

The HMMF model was successfully applied to lung CT segmentation and pulmonary emphysema quantification. The proposed method was shown to be robust with respect to the

Table 1. Mean values (M), standard deviations (SD), maximum values (Max), and minimum values (Min) of EI for different quantification methods, over 22 subjects.

Measure	M	SD	Max	Min
EI_{MF}^{31}	10.0	2.6	15.6	6.1
EI_{-980}^{31}	1.6	1.5	4.8	0.1
EI_{-950}^{31}	7.8	6.4	21.3	0.8
EI_{-910}^{31}	32.1	15.5	56.8	6.1
EI_{MF}^{46}	10.6	3.2	18.6	5.4
EI_{-980}^{46}	6.7	3.8	14.5	2.0
EI_{-950}^{46}	16.9	7.9	31.6	6.2
EI_{-910}^{46}	38.8	12.5	58.0	14.8

Table 2. Mean absolute differences \pm standard deviations (MAD), root mean square differences ($RMSE$), and maximum absolute differences ($MaxAD$) of EI between [B31f, B46f] and between [B31f, B60f] images from a single acquisition, for different quantification methods, over 22 subjects.

Measures	MAD	$RMSE$	$MaxAD$
$EI_{MF}^{31}/EI_{MF}^{46}$	1.1 ± 0.8	1.3	3.0
$EI_{-980}^{31}/EI_{-980}^{46}$	5.2 ± 2.5	5.7	9.7
$EI_{-950}^{31}/EI_{-950}^{46}$	9.0 ± 2.3	9.3	13.5
$EI_{-910}^{31}/EI_{-910}^{46}$	6.7 ± 3.3	7.4	11.5
$EI_{MF}^{31}/EI_{MF}^{60}$	2.1 ± 1.6	2.6	5.8
$EI_{-980}^{31}/EI_{-980}^{60}$	20.1 ± 4.1	20.5	26.5
$EI_{-950}^{31}/EI_{-950}^{60}$	23.6 ± 2.6	23.7	28.0
$EI_{-910}^{31}/EI_{-910}^{60}$	14.0 ± 7.7	15.9	25.7

noise level in the image, provided that the parameters of the model are given appropriate values. In particular, the Markov field weight λ needs to be tied to the image noise level and in this work it was assigned based on the reconstruction algorithm. In the future, we plan to use an adaptive value, selected based on a measure of the input image noise level.

Based on our results, it seems very likely that the commonly used methods for CT lung analysis based on fixed threshold values constantly either under- or overestimate the disease extent, given the amount of intensity variation present in the images. However, this study does not claim that the proposed method is able to provide a quantification that is closer to the “true” amount of emphysematous tissue. While this study showed robustness to noise resulting from the applied reconstruction kernels, the other key component of the HMMF-based approach, related to the adaptivity to variability in intensity distributions, will be the topic of the next study. In addition, showing correlation with histological findings and mortality remains a future aim to show that the results correspond to the true extent of the disease.

The use of a robust and reproducible automated method may have a significant impact on emphysema quantification, especially for longitudinal studies where imaging protocols change and patients’ ability to reach full inspiration may de-

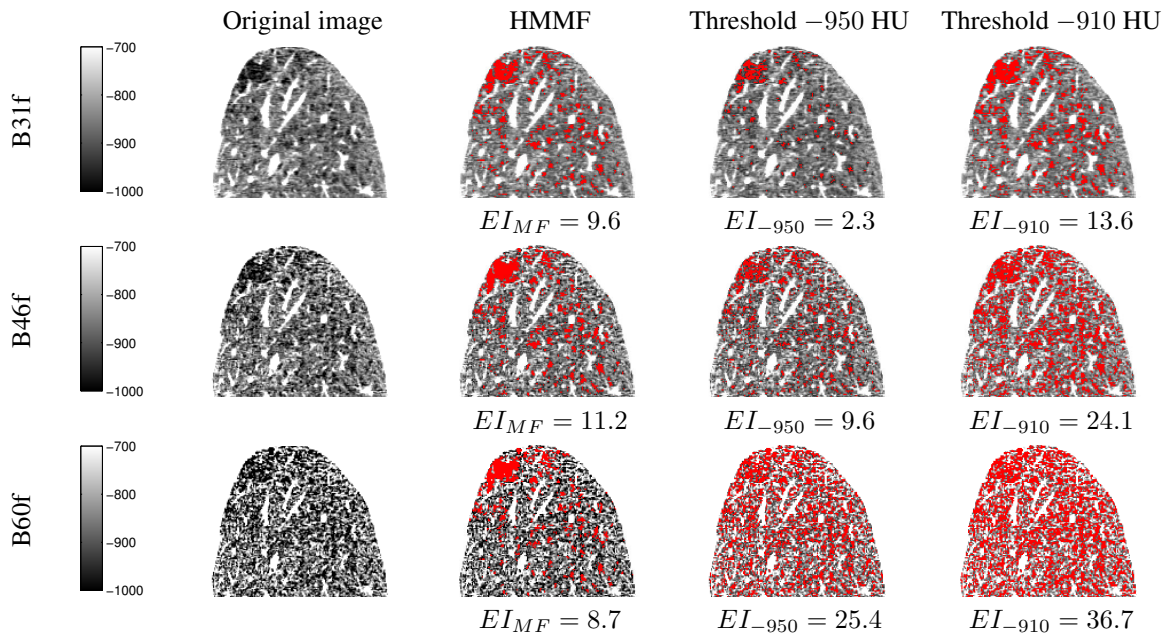


Fig. 2. Example of emphysema indices (EI) with different methods for a single acquisition reconstructed with three different kernels: B31f, B46f, and B60f (resulting scores are reported below each image). The images represent a cropped coronal slice of the CT volumes with windowing $[-1000, -700]$ HU. The overlaid red points correspond to voxels classified as emphysema. The columns correspond to different quantification methods and the rows correspond to different reconstruction kernels.

cline. In a future study, the proposed method will be applied on a large longitudinal dataset of COPD patients to show prediction capability of the method.

5. REFERENCES

- [1] O.M. Mets, P.A. de Jong, B. van Ginneken, H.A. Gietema, and J.W.J. Lammers, "Quantitative computed tomography in COPD: possibilities and limitations," *Lung*, pp. 1–13, 2012.
- [2] "Global initiative for chronic obstructive lung disease. Global strategy for the diagnosis, management, and prevention of chronic obstructive pulmonary disease," Updated 2011, accessed October 2012. Available at: <http://www.goldcopd.com>.
- [3] E.A. Hoffman, B.A. Simon, and G. McLennan, "State of the art. A structural and functional assessment of the lung via multidetector-row computed tomography phenotyping chronic obstructive pulmonary disease," *Proceedings of the American Thoracic Society*, vol. 3, no. 6, pp. 519–532, 2006.
- [4] M. Ceresa, G. Bastarrika, J.P. de Torres, L.M. Montuenga, J.J. Zulueta, C. Ortiz-de Solorzano, and A. Muñoz-Barrutia, "Robust, standardized quantification of pulmonary emphysema in low dose CT exams," *Academic Radiology*, vol. 18, no. 11, pp. 1382–1390, 2011.
- [5] S.T. Bartel, A.J. Bierhals, T.K. Pilgram, C. Hong, K.B. Schechtman, S.H. Conradi, and D.S. Gierada, "Equating quantitative emphysema measurements on different CT image reconstructions," *Medical Physics*, vol. 38, no. 8, pp. 4894, 2011.
- [6] L. Sorensen, M. Nielsen, P. Lo, H. Ashraf, J.H. Pedersen, and M. de Bruijne, "Texture-based analysis of COPD: A data-driven approach," *IEEE TMI*, vol. 31, no. 1, pp. 70–78, 2012.
- [7] Y. Xu, M. Sonka, G. McLennan, J. Guo, and E.A. Hoffman, "MDCT-based 3-D texture classification of emphysema and early smoking related lung pathologies," *IEEE TMI*, vol. 25, no. 4, pp. 464–475, 2006.
- [8] S.B. Ginsburg, D.A. Lynch, R.P. Bowler, and J.D. Schroeder, "Automated texture-based quantification of centrilobular nodularity and centrilobular emphysema in chest CT images," *Academic Radiology*, vol. 19, no. 10, pp. 1241–1251, 2012.
- [9] J.L. Marroquin, E.A. Santana, and S. Botello, "Hidden Markov measure field models for image segmentation," *IEEE TPAMI*, vol. 25, no. 11, pp. 1380–1387, 2003.
- [10] Y. Häme and M. Pollari, "Semi-automatic liver tumor segmentation with hidden Markov measure field model and non-parametric distribution estimation," *Medical Image Analysis*, vol. 16, no. 1, pp. 140–149, 2012.
- [11] R.G. Barr, S. Mesia-Vela, J.H.M. Austin, R.C. Basner, B.M. Keller, A.P. Reeves, D. Shimbo, and L. Stevenson, "Impaired flow-mediated dilation is associated with low pulmonary function and emphysema in ex-smokers the emphysema and cancer action project (EMCAP) study," *Am. J. Respir. Crit. Care Med*, vol. 176, no. 12, pp. 1200–1207, 2007.
- [12] S. Hu, E.A. Hoffman, and J.M. Reinhardt, "Automatic lung segmentation for accurate quantitation of volumetric X-ray CT images," *IEEE TMI*, vol. 20, no. 6, pp. 490–498, 2001.
- [13] Y. Masutani, K. Masamune, and T. Dohi, "Region-growing based feature extraction algorithm for tree-like objects," in *Visualization in Biomedical Computing*. Springer, 1996.